An R-matrix with pseudostates approach to the electron-impact excitation of H I for diagnostic applications in fusion plasmas

H Anderson, C P Ballance, N R Badnell and H P Summers

Department of Physics and Applied Physics, University of Strathclyde, Glasgow G4 0NG, UK

Abstract. Electron-impact excitation cross sections for transitions between terms up to the $n = 5$ shell of neutral hydrogen have been calculated using the R-matrix method with pseudostates and compared with previous studies. Maxwell-averaged effective collision strengths have been prepared and used in population calculations to examine effective emission coefficients for diagnostic applications in fusion plasmas. Our results remove an uncertainty in the reaction rates of an important class of atomic processes governing H I emission in plasmas.

1. Introduction

Spectral line observations of neutral hydrogen in plasmas are extensively used for diagnostic inference. In the fusion plasma regime, with moderate electron densities $\sim 10^{13}$ cm^{-3}, the collision limit approaches the $n = 4, 5$ quantum shells and so the line ratios such as H_γ/H_α and H_β/H_α are density diagnostic indicators. The hydrogen emission can occur from plasma of relatively high temperature (20 eV) at one extreme, and from plasma of very low temperature (0.5 eV) in the other extreme during detachment from divertor strike zones, depending on recycling and gas puffing procedures. At detachment, a transition from an excitation mechanism for the line formation to a volume recombination mechanism can also be evident in these line ratios (McCracken *et al* 1997). The precision of modelling of the effective emission coefficients is then strongly dependent on direct electron impact excitation cross sections from the 1s level to higher quantum shells $n = 3$–6 (especially in the high-temperature regime) and on stepwise cross sections such as $n = 3 \rightarrow 4$ and $n = 4 \rightarrow 5$ (especially in the low-temperature regime). It is precisely these data which have been historically least well known due to continuum flux issues in close-coupling calculations.

Electron-impact excitation of neutral hydrogen has been studied extensively using a variety of methods. These include the standard R-matrix approach (Aggarwal *et al* 1991), R-matrix with pseudostates (Bartschat *et al* 1996), the intermediate energy R-matrix approach (Scott *et al* 1989), as well as the variational close coupling methods of Callaway and co-workers (1987, 1988, 1993) and the convergent close coupling method of Bray and co-workers (1992a, b, 1999). Apart from Aggarwal *et al* (1991), these calculations have focused on transitions between the ground state and terms up to the $n = 3$ shell. An exception is Dunseath *et al* (1999) who have employed a novel two-dimensional R-matrix propagator technique to study resonance widths in a small energy band below 0.96 Ryd. However, in general, excitation data involving the $n = 3, 4, 5$ and 6 shells are sparse in energy or incomplete in transitions.

2. Calculation and results

The work of Aggarwal *et al* (1991) treats the first 15 terms without the inclusion of pseudostates. Although this provides accurate results below the ionization threshold, it can produce inflated cross sections above it. As discussed by Callaway and Unnikrishnan (1993), above the ionization threshold the inclusion of pseudostates is necessary to account for the loss of electron flux into the continuum. In this work, a comprehensive examination of the

$$ nl \rightarrow n'l' \quad n, n' \in \{1, 2, 3, 4, 5\} \quad l, l' \in \{0, 1, 2, 3, 4\} \quad n \neq n' \tag{1} $$

transitions was carried out using the *R*-matrix method with pseudostates. Particular attention was focused on producing a new set of benchmark results for transitions between the $3 \leqslant n \leqslant 5$ excited states of neutral hydrogen suited to moderate-density collisional–radiative population models. We have also noticed that although most of the lower-lying transitions have been investigated, the energy meshes used tended to be either piecewise or coarse. We therefore decided to use a fine energy grid (figure 1) across our entire range to ensure that all the resonance structure was fully delineated and the impact on the effective collision strengths appreciated.

The orbitals required to describe our discrete states, as well the pseudostates, were provided by AUTOSTRUCTURE (Badnell 1986). The 15 physical states (1s–5g) were supplemented by 24 pseudostates described by the $\bar{n}\bar{l}$ orbitals ($\bar{n} = 6\text{–}9$, $\bar{l} = 0\text{–}5$). These are regularly spaced in energy extending from the ionization threshold to 2 Ryd. Ideally, atomic modellers would like the inclusion of higher physical $n > 5$ shells, but it was found that physical $n = 6$ orbitals became so diffuse that the *R*-matrix box required to encapsulate such a charge cloud was approximately 140 a_0 in size. Prohibited by the computational demands of including these orbitals we decided to proceed with the 39-state model outlined above. To investigate the convergence of the pseudostate expansion, we carried out several calculations for a typical symmetry ($^1\text{H}^\text{o}$) varying the number of pseudostates both in $\bar{n}$ and $\bar{l}$. The results indicate that convergence in the cross section to within at least 10% was achieved with the 24-pseudostate model. Ionization cross sections were also obtained as a byproduct of the excitation cross section calculation. They showed broad agreement with Bray (1999).

The standard *R*-matrix package (Berrington *et al* 1995) was used to generate the scattering symmetries up to a maximum angular momentum of $L = 10$ allowing for the aforementioned pseudostates following Badnell and Gorczyca (1997). To account for an incident electron of higher angular momentum we employed the non-exchange *R*-matrix program (Burke *et al* 1992) for partial waves with L values between 11 and 70, the contribution from higher partial waves was found to be negligible. Both FARM (Burke and Noble 1995) and a neutral version of STGF (Badnell 1999) were used as outer-region packages and the resulting agreement of the collision strengths provided a check on the new version of STGF. Figure 1 shows the complete energy range from below ionization threshold to 27 eV for the 2s → 3p transition compared with the results of Bray (1999), Callaway *et al* (1987) and Aggarwal *et al* (1991), while figure 2 focuses on the detailed structure in the 12–13 eV energy range which cannot be clearly resolved in figure 1. Below the ionization threshold our results agree with those of Aggarwal *et al*, whilst above this threshold their results diverge due to continuum loss not being modelled. Callaway *et al* (1987) have given a few values over a sparse energy grid which agree well with both the results of Bray (1999) and those of our own present calculation. The shortcomings of the *R*-matrix method without pseudostates above 13.65 eV are most prominent for transitions between the $3 \leqslant n \leqslant 5$ shells, as illustrated in figure 3 for the 3d → 4d transition. The first three energy points of Aggarwal *et al* are in close agreement with present results but by 18 eV discrepancies are in excess of 30%. This pattern is continued (though it is more severe) amongst the transitions between the $n = 4$ and 5 shells.
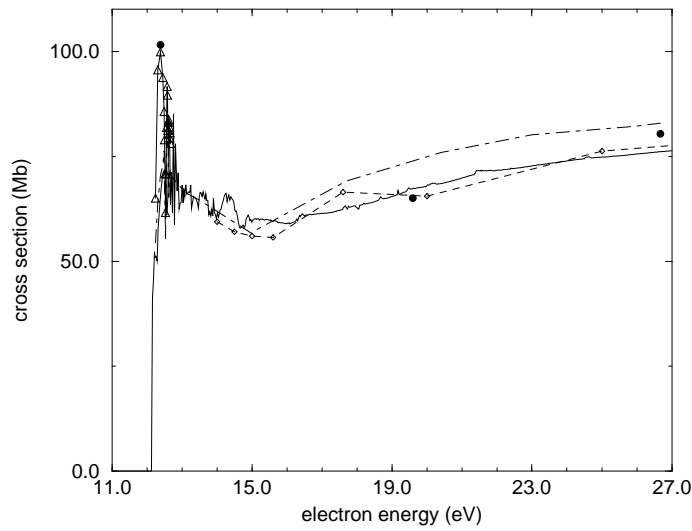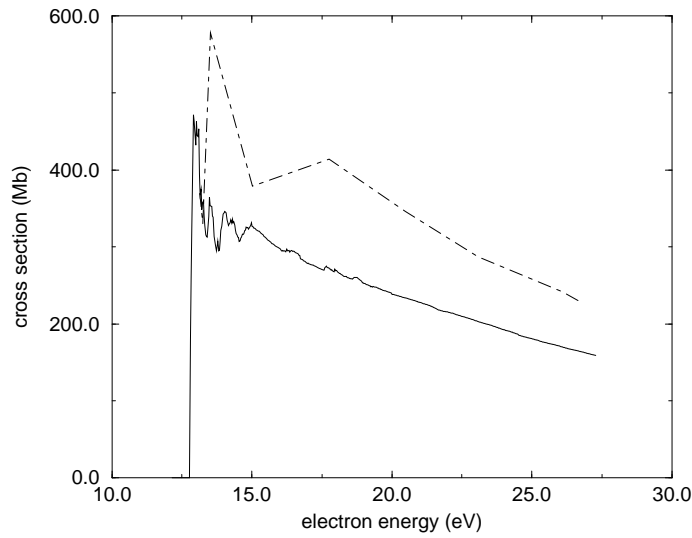
Figure 1. Electron-impact excitation cross section for the 2s $\rightarrow$ 3p transition in neutral hydrogen. The solid circles denote the results of Callaway *et al* (1987); the dashed curve, Aggarwal *et al* (1991); the dashed curve with diamonds, Bray (1999); the solid curve with triangles, Callaway (1988). The present results are denoted by the solid curve.
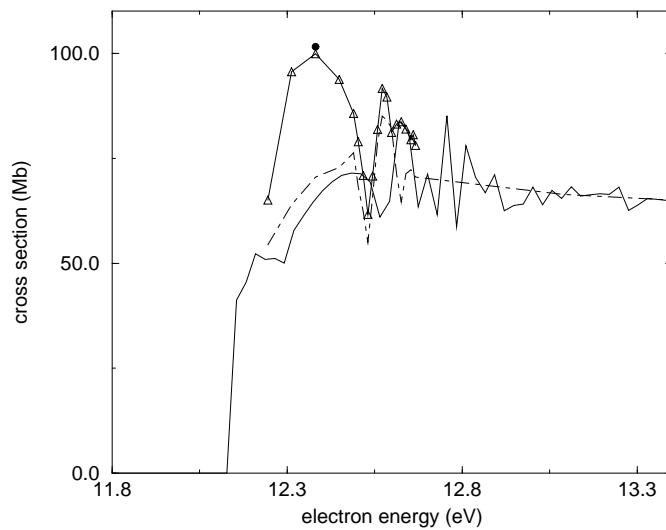
Figure 2. Below threshold electron-impact excitation cross section for the 2s $\rightarrow$ 3p transition in neutral hydrogen. The solid circles denote the results of Callaway *et al* (1987); the dashed curve, Aggarwal *et al* (1991); the solid curve with triangles, Callaway (1988). The present results are denoted by the solid curve.

3. Application of fundamental data

Detailed studies are now underway on the impact of the present new higher precision cross sections on hydrogen populations, ionization stage and spectral diagnostics at a number of fusion laboratories. These studies principally use the modelling tools and databases of the

Figure 3. Electron-impact excitation cross section for the 3d → 4d transition in neutral hydrogen. The dashed curve denotes the results of Aggarwal *et al* (1991). The present results are denoted by the solid curve.

Table 1. Term energies and indexing for H up to $n = 5$.

Term	*nl*	$2S + 1$	*L*	cm^{-1}
1	1s	2	0	0
2	2s	2	0	82 303
3	2p	2	1	82 303
4	3s	2	0	97 544
5	3p	2	1	97 544
6	3d	2	2	97 544
7	4s	2	0	102 879
8	4p	2	1	102 879
9	4d	2	2	102 879
10	4f	2	3	102 879
11	5s	2	0	105 348
12	5p	2	1	105 348
13	5d	2	2	105 348
14	5f	2	3	105 348
15	5g	2	4	105 348

Atomic Data and Analysis Structure, ADAS (Summers 1994, 1999). We have used ADAS to give a preliminary assessment of the sensitivity to the new data. Cross sections over the *R*-matrix energy grids were converted to Maxwell-averaged effective collision strengths using the utility *adasex* (Griffin 1998). The effective collision strength, Υ, is defined by the equation

$$\Upsilon_{ij} = \int_0^\infty \Omega(i \to j) \exp\left(\frac{-\epsilon_j}{kT_e}\right) d\left(\frac{\epsilon_j}{kT_e}\right), \tag{2}$$

where Ω is the collision strength for the transition from level i to level j and ϵ_j is the continuum energy of the final scattered electron. It is especially convenient for interpolation with respect to the electron temperature, T_e, because it has a much more gradual variation with temperature than that of the rate coefficient.

Table 2. Effective collision strengths for the $nl \rightarrow n'l'$ transitions in H for $n, n' \in \{1, 2, 3, 4, 5\}$, $l, l' \in \{0, 1, 2, 3, 4\}$ and $n \neq n'$.

			Electron temperature (eV)							
i	j	A_{ij}[a]	0.5	1.0	3.0	5.0	10.0	15.0	20.0	25.0
2	1	8.23+00[b]	2.60−01	2.96−01	3.25−01	3.37−01	3.56−01	3.68−01	3.75−01	3.80−01
3	1	6.27+08	4.27−01	5.36−01	8.57−01	1.15+00	1.75+00	2.13+00	2.35+00	2.46+00
4	1	0.00−00	6.45−02	6.89−02	7.72−02	8.06−02	8.33−02	8.41−02	8.45−02	8.46−02
5	1	1.67+08	1.11−01	1.26−01	1.86−01	2.40−01	3.13−01	3.29−01	3.20−01	3.04−01
6	1	0.00−00	6.17−02	6.56−02	7.81−02	8.98−02	1.10−01	1.22−01	1.29−01	1.35−01
7	1	0.00−00	2.13−02	2.51−02	3.18−02	3.38−02	3.48−02	3.48−02	3.47−02	3.46−02
8	1	6.82+07	3.81−02	4.70−02	7.39−02	9.41−02	1.23−01	1.33−01	1.32−01	1.28−01
9	1	0.00−00	2.87−02	3.12−02	4.02−02	4.72−02	5.74−02	6.28−02	6.60−02	6.82−02
10	1	0.00−00	1.18−02	1.11−02	1.05−02	1.06−02	1.11−02	1.16−02	1.18−02	1.20−02
11	1	0.00−00	1.40−02	1.69−02	1.91−02	1.92−02	1.88−02	1.85−02	1.83−02	1.82−02
12	1	3.44+07	2.60−02	3.12−02	4.04−02	4.74−02	5.71−02	5.82−02	5.58−02	5.23−02
13	1	0.00−00	2.01−02	2.18−02	2.47−02	2.75−02	3.15−02	3.35−02	3.46−02	3.53−02
14	1	0.00−00	8.79−03	8.87−03	9.42−03	9.95−03	1.09−02	1.14−02	1.17−02	1.19−02
15	1	0.00−00	4.36−03	3.86−03	2.79−03	2.35−03	1.88−03	1.65−03	1.51−03	1.42−03
4	2	0.00−00	1.39+00	1.47+00	2.29+00	3.06+00	4.26+00	4.89+00	5.28+00	5.54+00
5	2	2.25+07	2.42+00	3.07+00	5.31+00	7.79+00	1.38+01	1.91+01	2.36+01	2.76+01
6	2	0.00−00	2.05+00	3.10+00	6.59+00	9.30+00	1.35+01	1.57+01	1.71+01	1.80+01
7	2	0.00−00	3.75−01	3.80−01	5.05−01	6.29−01	8.23−01	9.27−01	9.91−01	1.03+00
8	2	9.67+06	7.28−01	8.89−01	1.45+00	1.95+00	3.06+00	3.98+00	4.76+00	5.43+00
9	2	0.00−00	6.30−01	7.45−01	1.12+00	1.40+00	1.83+00	2.05+00	2.19+00	2.28+00
10	2	0.00−00	5.43−01	7.33−01	1.29+00	1.63+00	2.09+00	2.31+00	2.44+00	2.52+00
11	2	0.00−00	1.90−01	2.07−01	2.31−01	2.59−01	3.13−01	3.45−01	3.65−01	3.78−01
12	2	4.95+06	4.01−01	5.10−01	7.13−01	8.75−01	1.28+00	1.64+00	1.97+00	2.25+00
13	2	0.00−00	4.16−01	4.76−01	5.52−01	6.02−01	6.81−01	7.23−01	7.50−01	7.67−01
14	2	0.00−00	3.75−01	4.55−01	6.75−01	8.16−01	9.92−01	1.07+00	1.12+00	1.15+00
15	2	0.00−00	2.28−01	2.49−01	2.50−01	2.47−01	2.46−01	2.45−01	2.45−01	2.45−01
4	3	6.32+06	2.00+00	2.18+00	2.26+00	2.33+00	2.64+00	2.96+00	3.26+00	3.54+00
5	3	0.00−00	7.18+00	7.90+00	1.07+01	1.32+01	1.71+01	1.92+01	2.05+01	2.13+01
6	3	6.47+07	1.31+01	1.81+01	3.73+01	5.64+01	9.81+01	1.32+02	1.59+02	1.83+02
7	3	2.58+06	6.92−01	7.43−01	7.47−01	7.33−01	7.35−01	7.61−01	7.93−01	8.26−01
8	3	0.00−00	2.06+00	2.20+00	2.67+00	3.05+00	3.63+00	3.94+00	4.13+00	4.25+00
9	3	2.06+07	3.40+00	4.30+00	7.65+00	1.07+01	1.69+01	2.16+01	2.53+01	2.84+01
10	3	0.00−00	2.62+00	3.18+00	4.93+00	6.10+00	7.71+00	8.52+00	9.01+00	9.32+00
11	3	1.29+06	4.48−01	5.00−01	4.71−01	4.34−01	3.87−01	3.64−01	3.47−01	3.35−01
12	3	0.00−00	1.26+00	1.37+00	1.36+00	1.38+00	1.46+00	1.52+00	1.56+00	1.59+00
13	3	9.43+06	1.99+00	2.46+00	3.45+00	4.31+00	6.16+00	7.59+00	8.75+00	9.72+00
14	3	0.00−00	1.65+00	1.99+00	2.90+00	3.48+00	4.23+00	4.59+00	4.80+00	4.93+00
15	3	0.00−00	8.13−01	8.89−01	9.10−01	8.90−01	8.46−01	8.18−01	7.99−01	7.86−01
7	4	0.00−00	2.57+00	4.38+00	1.09+01	1.52+01	2.12+01	2.42+01	2.59+01	2.71+01
8	4	3.07+06	4.32+00	6.09+00	1.54+01	2.58+01	4.89+01	6.72+01	8.23+01	9.50+01
9	4	0.00−00	6.21+00	1.02+01	2.30+01	3.22+01	4.55+01	5.24+01	5.65+01	5.93+01
10	4	0.00−00	6.63+00	1.06+01	1.97+01	2.48+01	3.14+01	3.47+01	3.67+01	3.79+01
11	4	0.00−00	9.87−01	1.57+00	2.91+00	3.55+00	4.31+00	4.66+00	4.87+00	5.00+00
12	4	1.64+06	2.50+00	3.43+00	5.57+00	7.34+00	1.11+01	1.41+01	1.66+01	1.87+01
13	4	0.00−00	3.22+00	4.17+00	6.12+00	7.07+00	8.29+00	8.90+00	9.26+00	9.49+00
14	4	0.00−00	2.80+00	3.33+00	4.10+00	4.45+00	4.81+00	4.95+00	5.02+00	5.07+00
15	4	0.00−00	3.63+00	4.77+00	6.72+00	7.87+00	9.38+00	1.01+01	1.05+01	1.08+01

Table 2. (Continued)

			Electron temperature (eV)							
i	j	A_{ij}[a]	0.5	1.0	3.0	5.0	10.0	15.0	20.0	25.0
7	5	1.84+06	3.90+00	4.83+00	7.63+00	9.72+00	1.36+01	1.66+01	1.90+01	2.11+01
8	5	0.00−00	1.37+01	2.08+01	4.51+01	6.16+01	8.42+01	9.54+01	1.02+02	1.06+02
9	5	7.04+06	2.06+01	3.21+01	8.33+01	1.35+02	2.42+02	3.25+02	3.91+02	4.46+02
10	5	0.00−00	2.47+01	4.13+01	8.83+01	1.19+02	1.62+02	1.83+02	1.96+02	2.05+02
11	5	9.05+05	2.14+00	2.52+00	2.99+00	3.23+00	3.72+00	4.15+00	4.52+00	4.84+00
12	5	0.00−00	7.11+00	9.60+00	1.39+01	1.58+01	1.82+01	1.93+01	2.00+01	2.05+01
13	5	3.39+06	1.10+01	1.52+01	2.67+01	3.55+01	5.18+01	6.36+01	7.29+01	8.07+01
14	5	0.00−00	9.95+00	1.23+01	1.64+01	1.82+01	2.01+01	2.08+01	2.12+01	2.15+01
15	5	0.00−00	1.42+01	1.84+01	2.47+01	2.87+01	3.43+01	3.71+01	3.88+01	3.99+01
7	6	0.00−00	3.97+00	4.13+00	4.30+00	4.54+00	4.94+00	5.16+00	5.30+00	5.38+00
8	6	3.48+05	1.31+01	1.52+01	1.96++01	2.17+01	2.43+01	2.57+01	2.66+01	2.73+01
9	6	0.00−00	3.31+01	4.58+01	8.31+01	1.07+02	1.40+02	1.56+02	1.65+02	1.71+02
10	6	1.38+07	6.38+01	1.15+02	3.30+02	5.22+02	8.89+02	1.15+03	1.36+03	1.53+03
11	6	0.00−00	2.64+00	2.83+00	2.50+00	2.25+00	1.96+00	1.84+00	1.77+00	1.73+00
12	6	1.50+05	7.81+00	8.63+00	8.67+00	8.46+00	8.31+00	8.38+00	8.50+00	8.64+00
13	6	0.00−00	1.61+01	2.06+01	2.72+01	2.93+01	3.16+01	3.26+01	3.32+01	3.37+01
14	6	4.54+06	2.75+01	4.00+01	7.83+01	1.06+02	1.50+02	1.78+02	1.99+02	2.15+02
15	6	0.00−00	2.88+01	3.84+01	5.33+01	6.19+01	7.48+01	8.16+01	8.58+01	8.86+01
11	7	0.00−00	6.62+00	1.61+01	4.35+01	5.72+01	7.20+01	7.83+01	8.18+01	8.40+01
12	7	7.38+05	9.63+00	1.77+01	4.28+01	6.27+01	1.01+02	1.31+02	1.56+02	1.78+02
13	7	0.00−00	1.39+01	2.56+01	6.18+01	8.38+01	1.11+02	1.24+02	1.31+02	1.35+02
14	7	0.00−00	2.16+01	3.47+01	6.31+01	7.64+01	9.08+01	9.69+01	1.00+02	1.02+02
15	7	0.00−00	1.96+01	2.74+01	4.12+01	4.75+01	5.47+01	5.79+01	5.98+01	6.10+01
11	8	6.45+05	1.07+01	1.80+01	2.95+01	3.40+01	4.10+01	4.65+01	5.13+01	5.56+01
12	8	0.00−00	3.83+01	7.60+01	1.76+02	2.25+02	2.79+02	3.02+02	3.15+02	3.23+02
13	8	1.49+06	4.00+01	7.17+01	1.88+02	2.80+02	4.48+02	5.71+02	6.70+02	7.53+02
14	8	0.00−00	6.74+01	1.15+02	2.42+02	3.14+02	4.02+02	4.42+02	4.65+02	4.80+02
15	8	0.00−00	6.71+01	9.86+01	1.63+02	1.95+02	2.33+02	2.50+02	2.59+02	2.66+02
11	9	0.00−00	1.21+01	1.57+01	1.89+01	2.01+01	2.17+01	2.24+01	2.29+01	2.32+01
12	9	1.89+05	4.04+01	5.98+01	8.39+01	8.90+01	9.21+01	9.35+01	9.48+01	9.63+01
13	9	0.00−00	8.75+01	1.60+02	3.36+02	4.17+02	5.02+02	5.36+02	5.54+02	5.65+02
14	9	2.59+06	1.05+02	2.00+02	5.43+02	8.15+02	1.30+03	1.65+03	1.92+03	2.15+03
15	9	0.00−00	1.65+02	2.61+02	4.81+02	6.09+02	7.73+02	8.50+02	8.95+02	9.24+02
11	10	0.00−00	9.63+00	1.05+01	9.45+00	8.68+00	7.81+00	7.43+00	7.22+00	7.09+00
12	10	0.00−00	3.33+01	3.96+01	3.94+01	3.69+01	3.35+01	3.19+01	3.10+01	3.04+01
13	10	5.05+04	7.24+01	1.02+02	1.31+02	1.30+02	1.16+02	1.04+02	9.46+01	8.76+01
14	10	0.00−00	1.62+02	2.70+02	5.29+02	6.52+02	7.76+02	8.24+02	8.50+02	8.65+02
15	10	4.26+06	3.81+02	7.45+02	1.77+03	2.47+03	3.62+03	4.42+03	5.03+03	5.53+03

[a] Dipole radiative rate.
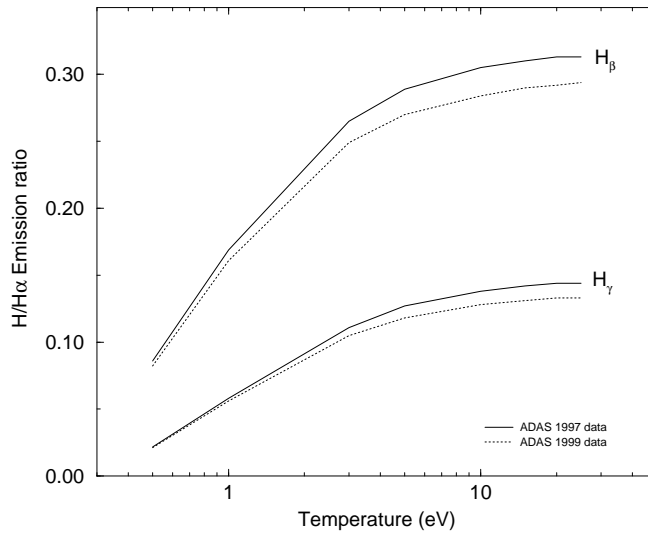[b] $a \pm b$ denotes $a \times 10^{\pm b}$.

The rate coefficients for collisional excitation $q_{i \to j}$ and de-excitation $q_{j \to i}$ can then be determined from the equations

$$q_{i \to j} = \frac{2\sqrt{\pi}\alpha c a_0^2}{\omega_i} \sqrt{\frac{I_H}{kT_e}} \exp\left(-\frac{\Delta E_{ij}}{kT_e}\right) \Upsilon_{ij}, \tag{3}$$

and

$$q_{j \to i} = \frac{\omega_i}{\omega_j} \exp\left(\frac{\Delta E_{ij}}{kT_e}\right) q_{i \to j}, \tag{4}$$

Figure 4. Partial effective H_γ/H_α emission ratio at $N_e = 5 \times 10^{12}$ cm^{-3}. The indirect contribution due to stepwise processes is denoted with the circles. The direct part is shown without circles. The dashed curves show the results obtained by using the existing ADAS electron collision data. These data include the work of Sampson *et al* (1983) for transitions amongst the excited states and the data of Callaway (1994) for the low-lying transitions. The present results are denoted by the solid curves.

where $2\sqrt{\pi}\alpha c a_0^2 = 2.1716 \times 10^{-8}$ cm^3 s^{-1}, $I_H = 13.6058$ eV, ΔE_{ij} is the threshold energy for the transition from level i to level j, and ω_i and ω_j are the statistical weights of level i and level j, respectively. These rate coefficients are calculated internally in ADAS from the values of the effective collision strengths. Our effective collision strengths are presented in table 2, with table 1 indexing the terms involved in our model.

Excited hydrogen populations, restricted to the first five principal quantum shells and omitting recombination, were calculated for $T_e = 0.5$–27 eV and $N_e = 5 \times 10^{12}$ cm^{-3} using the generalized collisional–radiative code *adas*205. Comparative results of the effective H_γ/H_α emission ratio are shown in figure 4. We have separated the contributions to the effective emission ratio due to direct excitation from the ground state and indirect stepwise processes. The direct contribution was obtained using *adas*205 while suppressing all the indirect collisional rates which enter into the model as input. The indirect contributions were obtained while individually suppressing the direct collisional rates from the ground state to the $n = 3$ and 5 shells.

The influence of the new collisional data on the direct contribution to the H_γ/H_α emission ratio is small. Differences between the behaviour of the new and the existing collisional data give rise to a crossing of the direct contribution at ≈ 3 eV. The sensitivity of the indirect contribution to the new data is more substantial and at 1 eV a difference of $\approx 14\%$ can be observed. The variation in individual cross sections between the old and new data can be as large as a factor of 2 but there is some cancellation in forming spectral emissivity ratios. The ratio of the direct contributions is most relevant to the high-temperature sensitivity while the ratio of the indirect part is most relevant to the low-temperature sensitivity in a finite-density fusion plasma. The sensitivity to the error in the cross sections of the indirect part decreases with increasing density as the collision limit falls. Note that a full solution for modelling fusion plasma requires a very many n-shell projection treatment including recombination and three-body processes.

4. Conclusion

We have generated benchmark collision cross section data for excitation between all terms of neutral hydrogen where $\Delta n > 0$ with $1 \leqslant n \leqslant 5$. The data have been converted to Maxwell-averaged effective collision strengths and archived within the ADAS database according to the data format *adf*04†. This work removes the uncertainty relating to the precision of electron-impact excitation data used in modelling the H I emission in plasmas.

References

Aggarwal K C, Berrington K A, Burke P G, Kingston A E and Pathak A 1991 *J. Phys. B: At. Mol. Opt. Phys.* **24** 1385
Badnell N R 1986 *J. Phys. B: At. Mol. Phys.* **19** 3827
——1999 *J. Phys. B: At. Mol. Opt. Phys.* **32** 5583
Badnell N R and Gorczyca T W 1997 *J. Phys. B: At. Mol. Opt. Phys.* **30** 2011
Bartschat K, Hudson E T, Scott M P, Burke P G and Burke V M 1996 *J. Phys. B: At. Mol. Opt. Phys.* **29** 115
Berrington K A, Eissner W B and Norrington P H 1995 *Comput. Phys. Commun.* **92** 290
Bray I 1999 *CCC On Line Database* webpage http://yin.ph.flinders.edu.au:8000/CCC-WWW/
Bray I and Stelbovics A 1992a *Phys. Rev. Lett.* **69** 53
——1992b *Phys. Rev.* A **46** 6995
Burke V M, Burke P G and Scott N S 1992 *Comput. Phys. Commun.* **69** 76
Burke V M and Noble C J 1995 *Comput. Phys. Commun.* **85** 471
Callaway J 1988 *Phys. Rev.* A **37** 3692
——1994 *At. Data Nucl. Data Tables* **57** 9
Callaway J and Unnikrishnan L 1993 *J. Phys. B: At. Mol. Opt. Phys.* **26** L419
Callaway J, Unnikrishnan L and Oza H 1987 *Phys. Rev.* A **36** 2576
Dunseath K M, Terao-Dunseath M, Le Dourneuf M and Launay J-M 1999 *J. Phys. B: At. Mol. Opt. Phys.* **32** 1739
Griffin D C 1998 Private communication
McCracken G M, Stamp M F, Monk R D, Meigs A, Lingertat, Prentice R, Starling A and Smith R 1997 *JET Joint Undertaking Report* JET-P(97)44
Sampson D H, Goett S J and Clark R E H 1983 *At. Data Nucl. Data Tables* **29** 467
Scott M P, Scholtz T T, Walters H R J and Burke P G 1989 *J. Phys. B: At. Mol. Opt. Phys.* **22** 3097
Summers H P 1994 *JET Joint Undertaking Report* JET-IR(94)06
——1999 *ADAS User Manual Version 2.1* webpage http:/patiala.phys.strath.ac.uk/adas/

† These data are also available directly from the authors.